**Advances in
Geosciences**

Simulation of polarimetric radar variables in rain at S-, C- and X-band wavelengths

F. Teschl[1], **W. L. Randeu**[1,2], **M. Schönhuber**[2], and **R. Teschl**[1]

[1]Department of Broadband Communications, Graz University of Technology, Graz, Austria
[2]Institute of Applied Systems Technology, Joanneum Research, Graz, Austria

Abstract. Polarimetric radar variables of rainfall events, like differential reflectivity Z_{DR}, or specific differential phase K_{DP}, are better suited for estimating rain rate R than just the reflectivity factor for horizontally polarized waves, Z_H. A variety of physical and empirical approaches exist to estimate the rain rate from polarimetric radar observables. The relationships vary over a wide range with the location and the weather conditions.

In this study, the polarimetric radar variables were simulated for S-, C- and X-band wavelengths in order to establish radar rainfall estimators for the alpine region of the form $R(K_{DP})$, $R(Z_H, Z_{DR})$, and $R(K_{DP}, Z_{DR})$. For the simulation drop size distributions of hundreds of 1-minute-rain episodes were obtained from 2D-Video-Distrometer measurements in the mountains of Styria, Austria. The sensitivity of the polarimetric variables to temperature is investigated, as well as the influence of different rain drop shape models – including recently published ones – on radar rainfall estimators. Finally it is shown how the polarimetric radar variables change with the elevation angle of the radar antenna.

1 Introduction

In polarimetric weather radar systems, relationships of the form $R(K_{DP})$, $R(Z_H, Z_{DR})$, and $R(K_{DP}, Z_{DR})$ are generally used to estimate the rain fall rate R. A wide range of relationships exist (e.g. Aydin and Giridhar, 1992; May et al., 1999; Keenan et al., 2001). The main reason for the wide range of relationships is the drop-size distribution. The drop-size distribution depends on the type of rain event and as a consequence on the geographical region. Also a variety of rain drop shape models exists and so the underlying rain drop

shape model has an influence on the determined rainfall algorithm as well (Matrosov et al., 2002).

At C-band also the temperature can have influence on the polarimetric rainfall estimation algorithms; for example, at 5 cm wavelength resonance occurs for sizes larger than about 5 mm diameter, and therefore several polarimetric observables exhibit non-monotonous dependence on the drop diameter (Zrnić et al., 2000). At C-band also a considerable temperature dependence of polarimetric observables can be observed, as described in Sect. 5. At X-band, resonance occurs for sizes around 4 mm but the temperature dependence is not significant.

In the present study, the polarimetric radar observables Z_H, Z_{DR}, and K_{DP} were calculated for 249 1-minute-rain episodes, observed with an imaging distrometer, the 2D-Video-Distrometer (Schönhuber et al., 1994), in the mountains of Styria, Austria.

2 Data

The raindrop-size distribution measurements were obtained from the 2D-Video-Distrometer positioned at Mt. Präbichl in the Province of Styria, Austria. The 2D-Video-Distrometer records front- and side-view as well as the time stamp of raindrops falling through its sensing area. The water volume of each rain drop and its equivolumetric sphere diameter is calculated from the recorded front- and side-view. The rain rate is determined from all particles that were falling through the effective measuring area in a certain integration time interval. The detailed algorithm is described in Schönhuber (1998). For this study 249 rain events were observed (Fig. 1). The analyzed data were recorded during convective and stratiform rainfall events in the years 2000 and 2001. The drop-size distribution was discretized in 0.25 mm steps of the equivolumetric sphere diameter D_{eq}, and averages over 1 min have been considered.

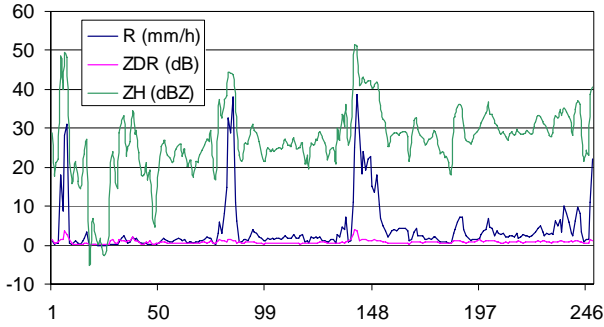*Correspondence to:* F. Teschl
(franz.teschl@tugraz.at)

Fig. 1. Rain rate R, reflectivity factor Z_H and differential reflectivity Z_{DR} as measured with the 2DVD for 249 rain episodes of 1 minute each. In this plot Z_H and Z_{DR} are determined for 5.625 GHz, 10°C, and assuming Pruppacher-Beard raindrop shapes.

3 Methodology

The forward- and backward-scattering amplitudes of single raindrops were calculated with the ESA point matching program (Poiares Baptista, 1994). It uses the point matching algorithm of Morrison and Cross (1974). The radar rain rate estimation algorithms of the form $R(K_{DP})$, $R(Z_H, Z_{DR})$ and $R(K_{DP}, Z_{DR})$ were established for S-, C- and X-band wavelengths by regression analyses, between the rain rate measured by the 2DVD and the calculated polarimetric radar variables for 249 1-minute-rain episodes, observed with the 2D-Video-Distrometer. In this study, the polarimetric variables K_{DP}, Z_H and Z_{DR} were calculated with following formulas:

$$K_{DP} = (180 \cdot 10^3) \frac{\lambda}{\pi} \cdot \mathrm{Re}$$

$$\int_{D=0}^{D\,\max} [f_{hh}(D) - f_{vv}(D)] \cdot N(D) \cdot dD \quad (^{\circ}\mathrm{km}^{-1}) \quad (1)$$

$$Z_H = \frac{4 \cdot 10^{18} \cdot \lambda^4}{\pi^4 \cdot \left|K_0^2\right| \cdot k^2} \int_{D=0}^{D\,\max} |s_{hh}(D)|^2 \cdot N(D) \cdot dD$$

$$(\mathrm{mm}^6 \ \mathrm{m}^{-3}) \quad (2)$$

$$Z_{DR} = \frac{\int_{D=0}^{D\,\max} |s_{hh}(D)|^2 \cdot N(D) \cdot dD}{\int_{D=0}^{D\,\max} |s_{vv}(D)|^2 \cdot N(D) \cdot dD} \quad (3)$$
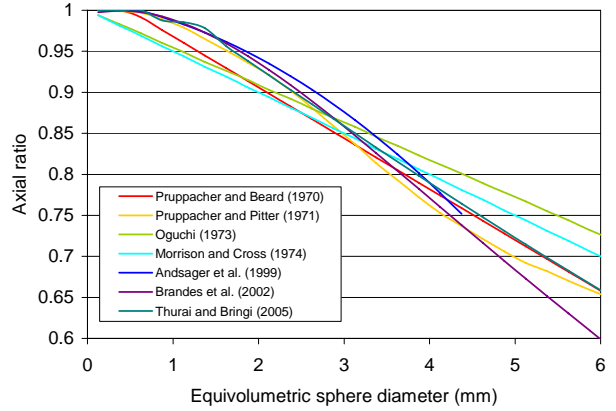

Fig. 2. Summary of several rain drop shape models showing the axial ratio of the drops as a function of the equivolumetric sphere diameter.

where

λ	wavelength (m)
k	propagation constant ($2\pi/\lambda$) (m^{-1})
$\left|K_0^2\right|$	material parameter, 0.931 for water
$N(D)$	drop-size distribution (mm^{-1} m^{-3})
D	drop diameter (mm)
$D_{\max}$	maximum drop diameter (mm)
Re	takes the real part of the integral
f_{hh}, f_{vv}	forward-scattering amplitudes for horizontally and vertically polarized waves (m)
s_{hh}, s_{vv}	backward-scattering amplitudes for horizontally and vertically polarized waves (m)

The forward and backward scattering amplitudes were calculated for 10°C raindrop temperature. The effect of temperatures between 0 and 30°C is also discussed. The complex relative dielectric permittivity ε of water was determined from Ray (1972). The calculations were carried out at S-band (2.8 GHz frequency/10.7 cm wavelength), C-band (5.625 GHz/5.3 cm) and at X-band (9.6 GHz/3.1 cm).

4 Raindrop shape models

The polarimetric variables are sensitive to the shape of the raindrops. In recent decades, a variety of different raindrop shape models were published and the research is still ongoing. Many of these models describe the full contour of the drops as a function of the equivolumetric sphere diameter. However, for practical applications the full contour shapes are often approximated by oblate spheroids with the same
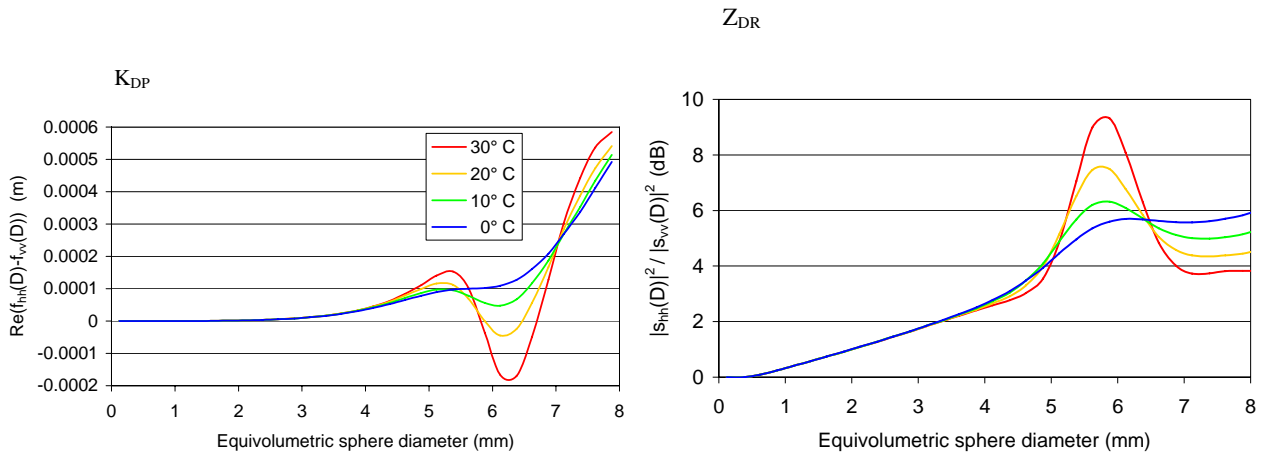
Fig. 3. K_{DP} and Z_{DR} as a function of equivolumetric sphere diameter of the raindrop, and temperature (at 5.3 cm wavelength).
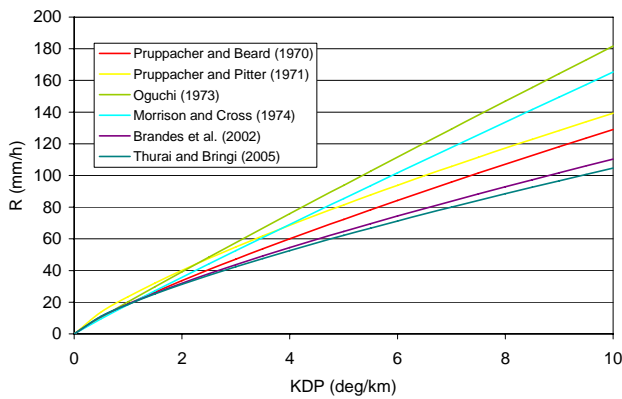

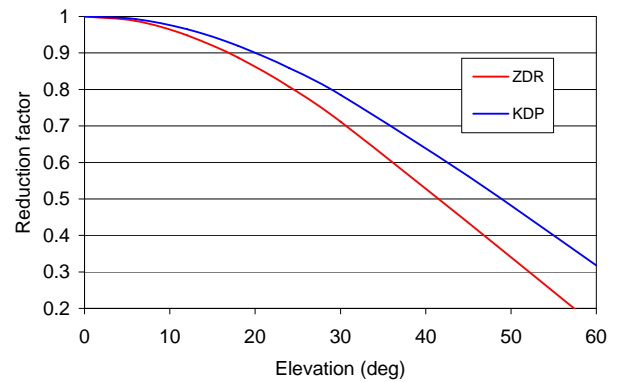**Fig. 4.** Comparison of the different $R(K_{DP})$ relationships at C-band.

Fig. 5. Reduction factor for K_{DP} and Z_{DR} with increasing elevation angle for Pruppacher-Beard rain drop shapes averaged over all observed drop-size distributions.

axial ratio. Figure 2 summarizes axial ratio relations of several models.

Polarimetric variables calculated from oblate spheroid approximations in general agree well with non-oblate shape models with equivalent axial ratio. Thurai at al. (2007) found noticeable deviation only within the resonance region for equivolumetric sphere diameters in the 5.5–7 mm range at C-band frequency. Since in our data only in two out of 249 different drop spectra rain drops in that range occurred, raindrops were also approximated by oblate spheroids.

5 Effect of raindrop temperature on K_{DP} and Z_{DR}

The effect of drop temperature on polarimetric radar variables has been studied e.g. by Bringi and Chandrasekhar (2001) and by Keenan et al. (2001). At S-band, effects of temperature on K_{DP} and Z_{DR} are rather small. At

C-band, however, effects of temperature are no longer negligible.

For equivolumetric sphere diameters up to 4 mm the temperature has no effect on K_{DP} and Z_{DR} while for bigger ones the effect can be significant as shown in Fig. 3. E.g. for 6 mm raindrops $\text{Re}(f_{hh} - f_{vv})$ turns negative at 20°C. This means that K_{DP} for a rain volume containing 6 mm drops can be less than the same volume without these drops.

This resonance effect occurs also for Z_{DR} and makes its use ambiguous at C-band frequency and around 6 mm drop diameter. Since in the analyzed distrometer data, 6 mm raindrops occurred only sporadically, no significant variation in the $R - K_{DP}$ relationship was observed at higher temperatures.

At X-band, the effect of the temperature is rather small. The resonance region resides just below 4 mm drop diameter and is not very pronounced.

Table 1. S-band rain rate estimation algorithms for different raindrop-shape models at 10°C. OG refers to Oguchi (1973), M&C refers to Morrison and Cross (1974), P&B refers Pruppacher and Beard (1970), P&P refers to Pruppacher and Pitter (1971). Units: R in mm h^{-1}, K_{DP} in °km^{-1}, Z_H in mm^6 m^{-3}, Z_{DR} in dB.

	S-band (2.8 GHz); ε_r=80.2346–j17.1513		
Shape model	$R(K_{DP})$algorithm	$R(K_{DP}, Z_{DR})$ algorithm	$R(Z_H, Z_{DR})$ algorithm
OG	R=41.14 $K_{DP}^{0.959}$	R=51.9 $K_{DP}^{0.98}10^{-0.082 ZDR}$	R=0.024 $Z_{H}^{0.90}10^{-0.769 ZDR}$
M&C	R=37.51 $K_{DP}^{0.959}$	R=47.4 $K_{DP}^{0.98}10^{-0.076 ZDR}$	R=0.024 $Z_{H}^{0.90}10^{-0.695 ZDR}$
P&B	R=35.33 $K_{DP}^{0.842}$	R=61.9 $K_{DP}^{0.91}10^{-0.176 ZDR}$	R=0.017 $Z_{H}^{0.90}10^{-0.565 ZDR}$
P&P	R=42.28 $K_{DP}^{0.779}$	R=86.4 $K_{DP}^{0.87}10^{-0.263 ZDR}$	R=0.015 $Z_{H}^{0.87}10^{-0.535 ZDR}$

Table 2. C-band rain rate estimation algorithms for different raindrop-shape models at 10°C. OG refers to Oguchi (1973), M&C refers to Morrison and Cross (1974), P&B refers Pruppacher and Beard (1970), P&P refers to Pruppacher and Pitter (1971), BR refers to Brandes et al. (2002), T&B refers to Thurai and Bringi (2005). Units: R in mm h^{-1}, K_{DP} in °km^{-1}, Z_H in mm^6 m^{-3}, Z_{DR} in dB.

	C-band (5.625 GHz); ε_r=70.46–j29.82		
Shape model	$R(K_{DP})$algorithm	$R(K_{DP}, Z_{DR})$ algorithm	$R(Z_H, Z_{DR})$ algorithm
OG	R=20.24 $K_{DP}^{0.953}$	R=25.9 $K_{DP}^{0.98}10^{-0.090 ZDR}$	R=0.022 $Z_{H}^{0.86}10^{-0.538 ZDR}$
M&C	R=18.46 $K_{DP}^{0.952}$	R=23.6 $K_{DP}^{0.98}10^{-0.082 ZDR}$	R=0.021 $Z_{H}^{0.86}10^{-0.483 ZDR}$
P&B	R=18.87 $K_{DP}^{0.835}$	R=29.1 $K_{DP}^{0.90}10^{-0.142 ZDR}$	R=0.017 $Z_{H}^{0.86}10^{-0.399 ZDR}$
P&P	R=23.49 $K_{DP}^{0.773}$	R=39.4 $K_{DP}^{0.85}10^{-0.197 ZDR}$	R=0.015 $Z_{H}^{0.84}10^{-0.377 ZDR}$
BR	R=18.77 $K_{DP}^{0.769}$	R=22.4 $K_{DP}^{0.77}10^{-0.072 ZDR}$	R=0.015 $Z_{H}^{0.82}10^{-0.290 ZDR}$
T&B	R=18.60 $K_{DP}^{0.750}$	R=24.4 $K_{DP}^{0.71}10^{-0.048 ZDR}$	R=0.016 $Z_{H}^{0.82}10^{-0.330 ZDR}$

6 Effect of raindrop shape models on radar rainfall estimation algorithms

Tables 1–3 summarize how different underlying rain drop shape models alter different radar rainfall estimation algorithms. The relationships were established in the same form as in Bringi and Chandrasekhar (2001). The results in this study are comparable to their findings when the different signal frequencies are taken in consideration. The results show that $R(K_{DP})$ algorithms are most affected by the used raindrop shape model. The estimated rain rate can vary significantly as seen in Fig. 4. For a maximum K_{DP} value in rain of 10 deg/km (Doviak and Zrnić, 1993), the C-band $R(K_{DP})$ algorithm reports a rain rate of 180 mm/h, when assuming the drop shape model of Oguchi (1973) in contrast to only 100 mm/h when assuming the model of Thurai and Bringi (2005). $R(K_{DP}, Z_{DR})$ algorithms are less affected than $R(K_{DP})$ esti-

mators; $R(Z_H, Z_{DR})$ algorithms are most robust to the axial ratio of the raindrops. The lowest rain rates arise when using the model of Pruppacher and Pitter (1971) or that of Brandes et al. (2002), the highest occur with the model of Pruppacher and Beard (1970).

7 Effect of the elevation angle on K_{DP} and Z_{DR}

The previous simulations were carried out assuming a radar beam parallel to the earth's surface. Below it is shown what effect elevation angles $>0°$ on the radar rainfall estimation algorithms have. For these simulations raindrop shapes according to Pruppacher and Beard (1970) were taken. With increasing elevation angle, K_{DP} and Z_{DR} decrease, because the raindrop shape seen by the radar becomes more spherical. Their decrease with increasing elevation is shown in Fig. 5.

Table 3. X-band rain rate estimation algorithms for different raindrop-shape models at 10°C. OG refers to Oguchi (1973), M&C refers to Morrison and Cross (1974), P&B refers Pruppacher and Beard , P&P refers to Pruppacher and Pitter (1971). Units: R in mm h^{-1}, K_{DP} in °km^{-1}, Z_H in mm^6 m^{-3}, Z_{DR} in dB.

X-band (9.6 GHz); ε_r=54.29–j38.17			
Shape model	$R(K_{DP})$ algorithm	$R(K_{DP}, Z_{DR})$ algorithm	$R(Z_H, Z_{DR})$ algorithm
OG	$R=11.91\ K_{DP}^{0.953}$	$R=14.5\ K_{DP}^{0.98}10^{-0.074ZDR}$	$R=0.023\ Z_H^{0.91}10^{-0.715ZDR}$
M&C	$R=10.88\ K_{DP}^{0.953}$	$R=13.2\ K_{DP}^{0.98}10^{-0.066ZDR}$	$R=0.023\ Z_H^{0.91}10^{-0.646ZDR}$
P&B	$R=11.84\ K_{DP}^{0.836}$	$R=17.7\ K_{DP}^{0.90}10^{-0.135ZDR}$	$R=0.016\ Z_H^{0.91}10^{-0.536ZDR}$
P&P	$R=15.30\ K_{DP}^{0.774}$	$R=25.11\ K_{DP}^{0.85}10^{-0.192ZDR}$	$R=0.014\ Z_H^{0.88}10^{-0.508ZDR}$

Table 4. C-band radar rain rate estimation algorithms for different elevation angles, for Pruppacher-Beard raindrop shapes and 10°C raindrop temperature.

C-band (5.625 GHz)			
Elevation angle	$R(K_{DP})$ algorithm	$R(K_{DP}, Z_{DR})$ algorithm	$R(Z_H, Z_{DR})$ algorithm
0°	$R=18.87\ K_{DP}^{0.835}$	$R=29.1\ K_{DP}^{0.90}10^{-0.142ZDR}$	$R=0.017\ Z_H^{0.86}10^{-0.399ZDR}$
6°	$R=19.04\ K_{DP}^{0.835}$	$R=29.4\ K_{DP}^{0.90}10^{-0.144ZDR}$	$R=0.017\ Z_H^{0.86}10^{-0.404ZDR}$
12°	$R=19.58\ K_{DP}^{0.835}$	$R=30.3\ K_{DP}^{0.90}10^{-0.150ZDR}$	$R=0.017\ Z_H^{0.86}10^{-0.420ZDR}$
18°	$R=20.52\ K_{DP}^{0.835}$	$R=32.0\ K_{DP}^{0.90}10^{-0.160ZDR}$	$R=0.017\ Z_H^{0.86}10^{-0.449ZDR}$
24°	$R=21.96\ K_{DP}^{0.835}$	$R=34.5\ K_{DP}^{0.90}10^{-0.176ZDR}$	$R=0.017\ Z_H^{0.86}10^{-0.493ZDR}$
30°	$R=23.99\ K_{DP}^{0.835}$	$R=38.2\ K_{DP}^{0.90}10^{-0.199ZDR}$	$R=0.017\ Z_H^{0.86}10^{-0.558ZDR}$

The curves represent an average over all observed drop-size distributions and is nearly identical at S-, C- and X-band.

The reduction factors obtained are:

$$Red_{KDP}(\gamma)=1+6.3\ 10^{-4}\gamma-3.2\ 10^{-4}\gamma^2+2\ 10^{-6}\gamma^3 \quad (4)$$

for K_{DP} and

$$Red_{ZDR}(\gamma)=1+3.6\ 10^{-4}\gamma-4.2\ 10^{-4}\gamma^2+3\ 10^{-6}\gamma^3 \quad (5)$$

for Z_{DR}. (The elevation angle γ is in degrees.) The formulas are valid for S-, C- and X-band and for elevation angles up to 60°.

Table 4 gives the rainfall estimation algorithms for elevation angles up to 30°.

8   Conclusions

In this study, the polarimetric radar variables Z_H, K_{DP} (specific differential phase) and Z_{DR} (differential reflectivity) were calculated for measured drop-size spectra for S-, C- and X-band wavelengths and radar rainfall estimation algorithms for the alpine region of the form $R(K_{DP})$, $R(Z_H, Z_{DR})$, and $R(K_{DP}, Z_{DR})$ were found.

It could be shown that different raindrop-shape models could alter K_{DP} in the calculation by more than 25% and therefore can also account for a wide range of $R - K_{DP}$ relationships. The estimated rain rate can vary significantly for a given K_{DP} value when comparing the established shape models. The results also show that at C-band the raindrop temperature can influence K_{DP} strongly if the radar volume contains a significant number of raindrops >5 mm. As K_{DP} measurements are often noisy, especially at S- and C-band (Matrosov et al., 2002), $R(K_{DP})$ estimators are mainly stable at high rain rates with big drop sizes. Especially for such cases the effect of temperature on K_{DP} cannot be neglected. It was found that $R(Z_H, Z_{DR})$ algorithms are most robust to the axial ratio of the raindrops.

References

Andsager, K. K, Beard, V., and Laird, N. L.: Laboratory Measurements of axis ratios for large raindrops, J. Atmos. Sci., 56, 2673–2683, 1999.

Aydin, K. and Giridhar, V.: C-band Dual Polarization Radar Observables in Rain, Journal of Atmospheric and. Oceanic Technology, 9, 383–390, 1992.

Brandes, E., Zhang, G., and Vivekanandan, J.: Experiments in rainfall estimation with a polarimetric radar in a subtropical environment, J. Appl. Meteor., 41, 674–685, 2002.

Bringi, V. N. and Chandrasekhar, V.: Polarimetric Doppler Weather Radar, Principles and Applications, Cambridge University Press, 636 pp., 2001.

Doviak, R. J. and Zrnić, D. S.: Doppler Radar and Weather Observations – 2nd edition, Academic Press, San Diego, 1993.

Keenan, T. D., Carey, L. D., Zrnić, D. S., and May, P. T.: Sensitivity of 5 cm wavelength polarmetric radar variables to raindrop axial ratio and dropsize distribution, J. Appl. Meteor., 40, 526–545, 2001.

Matrosov, S. Y., Clark, K. A., Martner, B. E., and Tokay, A.: X-band polarimetric radar measurements of rainfall, J. Appl. Meteor., 41, 941–952, 2002.

May, P. T., Keenan, T. D., Zrnić, D. S., Carey, L. D., and Rutledge, S. A.: Polarimetric radar measurements of tropical rain at a 5-cm wavelength, J. Appl. Meteor., 38, 750–765, 1999.

Morrison, J. A. and Cross, M. J.: Scattering of a plane electromagnetic wave by axisymmetric raindrops, Bell Syst. Tech. J., 53, 955–1019, 1974.

Oguchi, T.: Attenuation and phase rotation of radio waves due to rain: Calculations at 19.3 and 34.8 GHz, Radio Sci., 8, 31–38, 1973.

Poiares Baptista, J. P. V.: OPEX reference book on radar – Second Workshop of the OLYMPUS propagation Experimenters, 8–10 November 1994, ESA ESTEC, Noordwijk, The Netherlands, ESA WPP publications, WPP-083, ISSN 1022–6656, 1994.

Pruppacher, H. R., and Beard, K. V.: A wind tunnel investigation of the internal circulation and shape of water drops falling at terminal velocity in air, Quart. J. Roy. Meteor. Soc., 96, 247–256, 1970.

Pruppacher, H. R. and Pitter, R. L.: A semi-empirical determination of the shape of cloud and rain drops, J. Atmos. Sci., 28, 86–94, 1971.

Ray, P. S.: Broadband complex refractive indices of ice and water, Appl. Opt. 11, 1836–1844, 1972.

Schönhuber, M., Urban, H., Poiares Baptista, J. P. V., Randeu, W. L., and Riedler, W.: Measurements of Precipitation Characteristics by a New Distrometer. Proceedings of Atmospheric Physics and Dynamics in the Analysis and Prognosis of Precipitation Fields, 15–18 November 1994, Rome, Italy, 1994.

Schönhuber, M.: About Interaction of Precipitation and Electromagnetic Waves, Doctoral thesis, Institute of Communications and Wave Propagation, Graz University of Technology, Austria, 1998.

Thurai, M., Huang, G. J., Bringi, V. N., Randeu, W. L., and Schönhuber, M.: Drop Shapes, Model Comparisons, and Calculations of Polarimetric Radar Parameters in Rain, J. Atmos. Ocean. Tech., 24, 1019–1032, 2007.

Thurai, M. and Bringi, V. N.: Drop Axis Ratios, from a 2D-Video Disdrometer, J. Atmos. Ocean. Technol., 22, 963–975, 2005.

Zrnić, D. S., Keenan, T. D., Carey, L. D., and May, P.: Sensitivity analysis of polarimetric variables at a 5-cm wavelength in rain, J. Appl. Meteor., 39, 1514-1526, 2000.